Final submitted version of

Micheletti, N., Tonini, M. and Lane, S.N., 2017. Geomorphological activity at a rock glacier front detected with a 3D density-based clustering algorithm. Geomorphology, 278, 287-97

https://www.sciencedirect.com/science/article/pii/S0169555X16305980

A 3-D clustering approach for feature detection from point clouds: application to a rock glacier front in the Swiss Alps

Abstract

Acquisition of high density point clouds using Structure from Motion photogrammetry and terrestrial laser scanners (TLS) has become commonplace in geomorphic science. However, the derived point clouds are often filtered and/or interpolated onto regular grids and the grids compared so as to detect change (erosion/deposition). This procedure is necessary for some applications (e.g. digital terrain analysis) but it leads to a considerable loss of potentially valuable information contained within the point clouds. In the present study, a semiautomatic method for geomorphological analysis and feature detection from point clouds is developed. An approach based on the Density-Based Spatial Clustering of Applications with Noise (DBSCAN) is applied to TLS data for a rock glacier front in the Swiss Alps. The proposed methods allowed the isolation of clusters of erosion and deposition directly from point clouds without the prior need for interpolation or data reduction and with an accuracy that depends only on the actual sampling resolution. The results are illustrated for the summer of 2015, a season of enhanced geomorphic activity associated with exceptionally high temperatures.

Keywords

DBSCAN, Terrestrial laser scanner, point clouds, feature detection, rock glacier

1 Introduction

The rapid development of new remote sensing methods for topographic measurement has revolutionized geoscience research over the last two decades. Central to many of these methods is the production of point clouds, often with an exceptionally high, but spatially variable point density. For instance, terrestrial laser scanning (TLS) has been one of the most successful method for 3D data collection in the geosciences \cite{Alho2009,Bauer2003,Deems2013,Gabbud2015,Glenn2006,Heritage2007,Schaefer2010} and by sequential acquisition can be used to detect and quantify surface change \cite{Abellan2014,Gabbud2015}.

Whilst the developments of terrestrial scanners and ground-based Structure from Motion photogrammetry have made data collection more cost effective as compared with airborne methods, three challenges arise. First, the large number of points acquired is computationally challenging, and datasets have to be filtered such that only a subset of points is finally retained for the analysis (e.g. \cite{Abellan2006}). The consequences of this dataset reduction are dependent on the spatial scales

of variability in the surfaces being considered and the questions being asked with those data. It is possible to reduce data density significantly without statistically altering the terrain proprieties at certain (coarser) scales \cite{Chaplot2001,Gessler2000}. However, representation of more detailed micro-scale topographic characteristics will need to retain a higher density of data points \cite{Florinsky2000,Anderson2006}. If the questions being asked of a dataset relate to change detection (i.e. determination of erosion and deposition), the scale chosen for the analysis will affect directly the estimations of changes obtained \citep{Lane1994}. Second, whilst unmanned airborne vehicles increasingly allow for low cost aerial survey, terrestrial data collection methods remain important but suffer from perspective effects, which can lead to either zones of occlusion (shadow effect) or spatially-variable point densities. For change detection, such zones need to be treated carefully. Third, in the vast majority of contributions (e.g. \cite{Alho2009,Gabbud2015,Jaboyedoff2012}) 3D point clouds are interpolated to digital elevation models (DEMs), either as regular raster grids or triangulated irregular networks (TINs). These are effectively 2.5D representations of the topography \cite{Jaboyedoff2012}) because they assign a single Z elevation to a point (defined by X, Y coordinates), excluding the possibility that the point has multiple Z values. Furthermore, rasterized DEMs will require very high grid densities to capture the detail available in the original point data, but DEMs created at high resolution will have areas highly dependent upon point interpolation processes, where the point cloud densities are lower. TINs have similar problems where large triangles are created in zones of low point density.

For these reasons, it may be appropriate to develop change detection methods based upon the direct analysis of the point clouds using semi-automatic or automatic methods to detect and extract individual features. The latter have been proposed recently, notably for rockfall detection and rock mass structure analysis \cite{Brodu2012,Gigli2011,Olsen2015,Riquelme2014,Rohmer2015,Tonini2014}and they tend to be based upon the identification of clusters of points that share the same characteristics. There are fewer examples of the application of cluster-based methods for volume calculation (e.g. \cite{Olsen2015}), especially where there has been no prior interpolation.

The aim of this paper is to develop and to apply a semi-automated method for isolating and identifying erosion and deposition features directly from point cloud data using a 3D-clustering algorithm. Specifically, we tested the Density-Based Spatial Clustering of Applications with Noise (DBSCAN, \cite{Ester1996}) for isolating single erosion and deposition features from a TLS-generated point cloud. This approach has been previously employed to quantification of rockfalls and detection of mass joints \cite{Riquelme2014, Tonini2014}. The novelty of the proposed approach consists in the implementation of the DBSCAN 3D-module for the direct detection and quantification of erosion and deposition from point clouds, without the need for interpolation and so avoiding the creation of associated artefacts. The only parameter that then influences the features detected is the density of the original TLS data. We developed the method for a classic example of a geomorphic system that has been studied using TLS (e.g. \cite{Bauer2003, Bodin2008, Avian2009}): rock glaciers.

2 Case study: the Tsarmine rock glacier

The proposed methodology was developed for a very active rock glacier front located in the Swiss Alps: the Tsarmine rock glacier. Generally speaking, active rock glaciers act as sediment conveyors

able to transfer large quantities of rock debris downward by permafrost-related creep \cite{Delaloye2010,GartnerRoer2012}. Their velocities may vary from a few centimeters to several meters per year \cite{Barboux2014,Lambiel2008}. Alpine rock glaciers are widely recognized as a primary agent in gravitational processes, including rockfalls and debris flows, as a result of their steep and unstable fronts \cite{Harris2009,Kaab2007,Lugon2010}. As a consequence, monitoring and quantifying their dynamics is of great interest, particularly in the face of climate change that could potentially enhance downslope displacement rates (e.g. \cite{Kaab2007,Lugon2010,Micheletti2015}).

The Tsarmine rock glacier is located in the H\'erens Valley, in the Western Swiss Alps (Figure \ref{location}). Its front is located at 2480 m a.s.l. (near the regional lower limit of permafrost \cite{Lambiel2001}) and it is steep, devoid of vegetation and unstable. From the front, there is the regular detachment of debris, with delivery to a steep corridor containing a small stream, where deposits of boulders are visible for several hundred meters downstream.

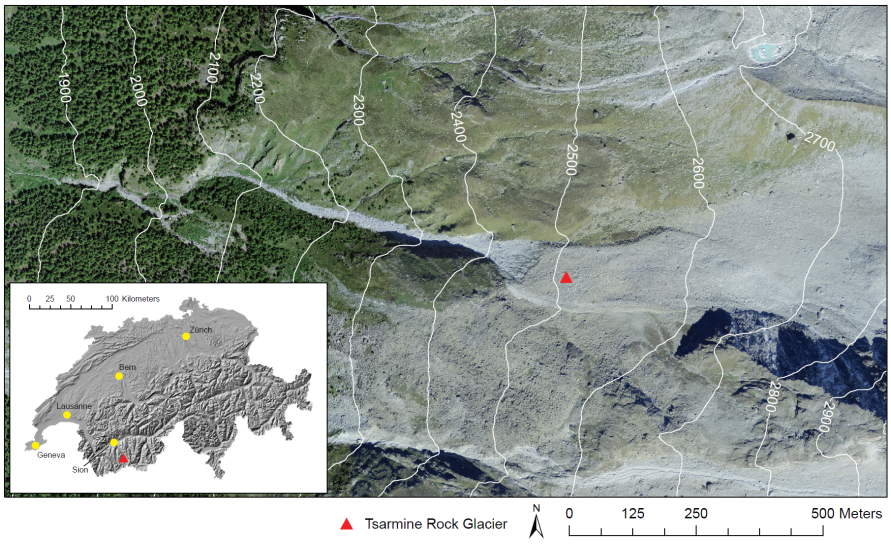

Figure 1. The Tsarmine rock glacier, located in the H\'erens Valley, in the Western Swiss Alps (aerial photograph and relief shaded: Swisstopo).

The kinematics of the Tsarmine rock glacier have been investigated using archival aerial photogrammetry, differential SAR interferometry (DInSAR), differential GPS and fixed GPS measurements \cite{Barboux2014,Delaloye2010,Lambiel2008,Micheletti2015}. Rapid creep, of the order of 1 to 2 myr^{-1}, was measured during the years 1990s and 2000s \citep{Barboux2014,Micheletti2015}. Following the rock glacier classification proposed by Lambiel (2008), the Tsarmine rock glacier might be considered very rapid and susceptible to very frequent destabilization. Recent GPS data suggest an apparent acceleration since the summer of 2012 and the body of the rock glaciers advanced at velocities of c. 4 myr^{-1} in the last years, with peaks up to 6 myr^{-1} in 2015 (unpublished data, Universities of Lausanne and Fribourg). Because of this exceptionally high displacement rate, the Tsarmine rock glacier is likely to be associated with considerable geomorphic change at its front even over short time-scales. As a consequence, it represents an ideal candidate for developing our method.

3 Methodology

Figure 2 gives an overview of the methodology, from data acquisition through to computation of the volume of change associated with each detected movement units (i.e. erosion and deposition features). In summary: (1) point clouds were generated using a TLS on a number of dates (see Tab.1); (2) these clouds were co-registered using stable zones within the surveyed area (bedrock outcrops); (3) the precision of the co-registration of the target dataset onto the reference dataset was used to define points where there may have been some change (erosion or deposition), expressed as a minimum Euclidean distance; (4) points that are retained were subjected to a clustering algorithm, DBSCAN, which aimed to group points into single features; (5) these features are then labeled as clusters of erosion or of deposition according to the elevation assignment of the change; and (6) the volume of change is finally calculated for each cluster.

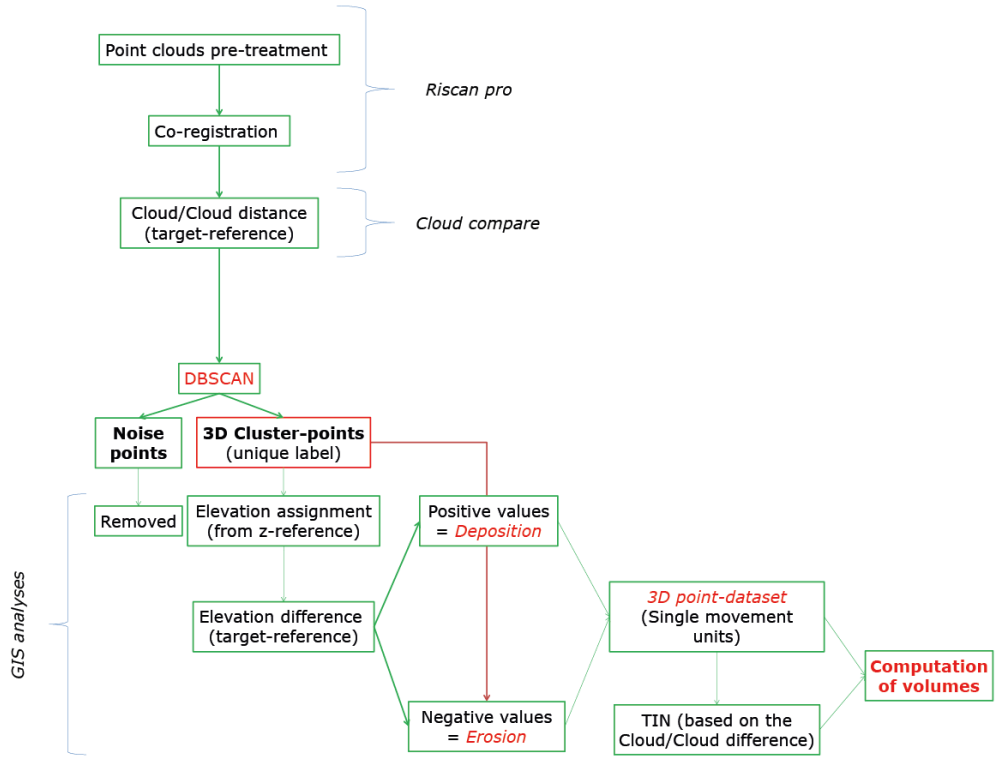

Figure 2: The workflow of the stepwise analysis for a single time-step. For each time-step analyzed, the target and reference point clouds are defined as shown in Table 1.

3.1 DBSCAN: 3-D density based clustering method

The clustering algorithm DBSCAN (*Density-Based Spatial Clustering of Applications with Noise, \cite{Ester1996,Campello2013}*) was used to classify points within the clouds into single cluster features. The computational environment to perform the analysis was the open source R programming language (R Core Team, 2015), using the dbscan package (Hahsler et al. 2016). This

procedure allows identification of clusters of arbitrary shape in 2D or 3D space on the base of the local density of points. Essentially, points that are close together are grouped into the same cluster, while points isolated or in very low-density regions are labelled as noise. Only two parameters are required to perform this classification: the neighborhood size epsilon (*eps*) and the minimum number of points necessary to form a cluster (*MinPts*). On the basis of these two parameters, the algorithm explores each point in the cloud, counting the number of the neighboring points falling within a circle (for the 2D model) or a sphere (for the 3D model) of radius equal to the *eps*-value: if this number is equal to or greater than the *MinPts*-value, the group of points is labeled as a *cluster*; otherwise the point is classified as *noise*. The central point of each identified cluster is called the *core*-point. Then, as some points in the pattern can be density-reachable by more than one *core*-point, they belong to more than one cluster. These are called *seed*-points. The corresponding *core*-points of clusters connected by seed points are said to be density-connected to each other and their clusters blended together to form a unique cluster of arbitrary shape.

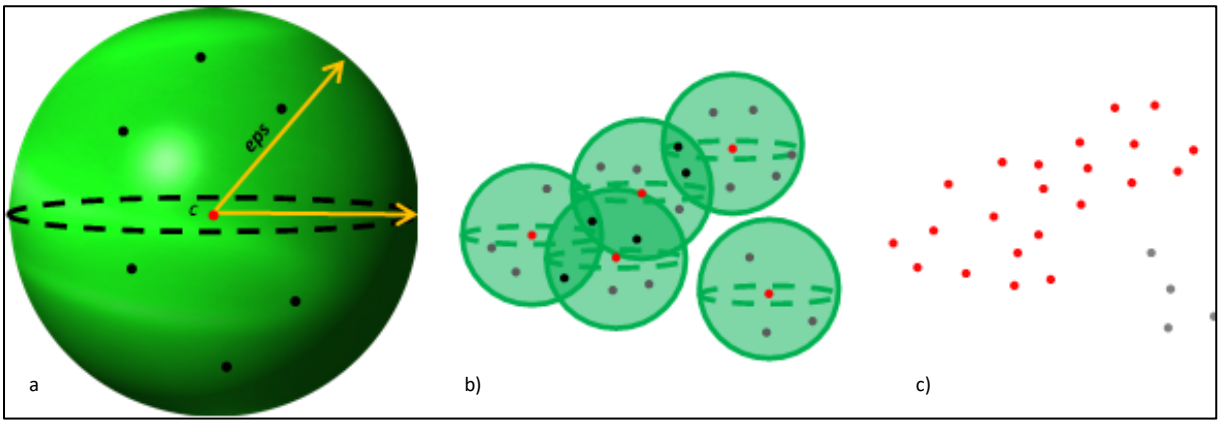

Figure 3: (a) The minimum number of points (*MinPts*) at a maximum distance (*eps*) around the core-point (*c,* red dots) defines a cluster. (b) The core-points are density-connected by the chain of intermediate seed-points, (black dots) and (c) their clusters (i.e. the reachable points) blended together to form a unique cluster of arbitrary shape (red point cloud).

The two parameters *eps* and *MinPts* greatly affect the shape, size and number of clusters detected by the algorithm. Their choice mainly relies on a decision that has to be taken as to whether the aim is to identify a large number of small clusters or a small number of large clusters within the original dataset. The default value for *MinPts* in the used package is 5 (Campello 2013). The actual value used should reflect: (1) dataset size, as when working with very high density datasets, higher values may need to be set to remove noise; and (2) the surface being considered which will determine the spatial scale of erosion and deposition units, and hence the point density that should be needed for a group of points to be coherent. Once that the *MinPts* parameter has been fixed**,** a suitable value for the *eps* neighborhood size can be deducted using a k-nearest-neighbours (k-NN) distance graph, that is plotting the distance to the k-nearest neighbour and imposing *k* as equal to *MinPts*. The optimal *eps*-value should coincide with strong curvature in the plot: smaller values should give rise to a strong fragmentation and small isolated clusters dispersed among noise-points; for larger values, the majority of the detected clusters will blend together to make bigger clusters.

3.2 Field campaign

An ultra-long range LiDAR RIEGL VZ-6000 scanner was employed to acquire sequential 3D datasets of the rock glacier front. This high speed (up to 222,000 measurements per second), high precision (10 mm at 150 m range) device has proven very efficient for geomorphological research (e.g. \cite{Fischer,Gabbud2015}). By means of its long-range (up to 6000 m) capability, the use of this device allowed the scan position to be set on the opposite side of the valley facing the rock glacier (c. 2800 m of flying distance,see Figure \ref{picture}). TLS scans were performed on four different dates over two consecutive summers: a first survey was carried out on the 23th of September 2014, whilst three more were completed on the 29th of June, the 20th of July and the 22th of September 2015. As it is routine in TLS surveys, the laser device was placed on a tripod over stable ground. The same approximate instrument position was used for each survey. The laser pulse repetition frequency was reduced to its minimal value (30 kHz) to prevent range ambiguity. Vertical and horizontal angle increments were both set to 0.004\degree, except for the 2014 survey where a value of 0.0045\degree was chosen (resulting in slightly lower expected point densities). For registration purposes, a very large area containing extensive stable zones in addition to the rock glacier was scanned. The RIEGL VZ-6000 is equipped with on-board inclination sensors, meaning that even when not geo-referenced, resulting data Z dimension represents the elevation above the X-Y plane. An example of the point cloud appearance at the rock glacier front is shown in Figure \ref{pointcloudfront}

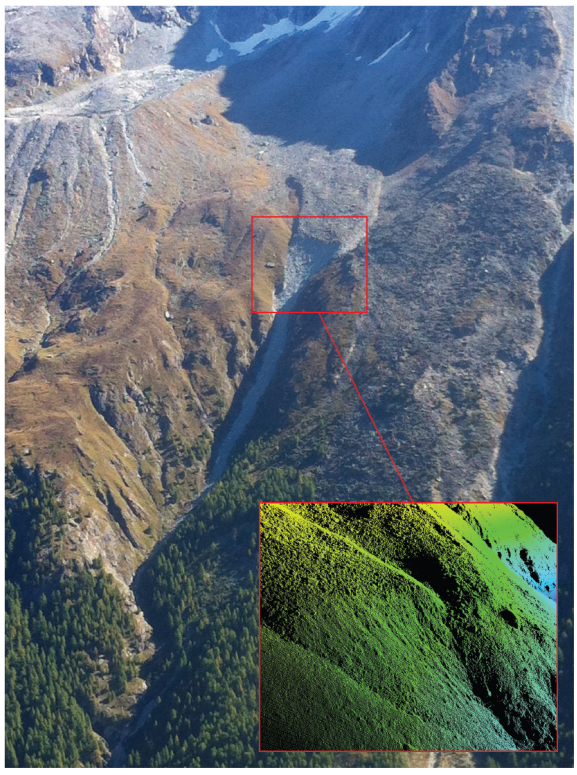

Figure 4. The Tsarmine rock glacier and the steep corridor below its front, as visible from the scanning site on the opposite valley side. The detail shows the point cloud of the rock glacier front (survey: 22/09/2015); the front width is c. 100 m.

3.3 Point cloud pre-treatment and co-registration

TLS data were imported and processed initially using the software RiSCAN PRO. The first step was manual removal of non-ground surface points, caused by atmospheric reflections due to dust or moisture. Afterwards, a relative registration of point clouds was necessary to co-register the four surveys into a common coordinate system. The most recent data (the 22th of September 2015) were treated as the datum.

Surfaces prone to considerable topographic change (including the rock glacier) were identified and excluded from the co-registration procedure. A coarse, approximate registration was achieved by manually identifying corresponding points between the datum and each point cloud and shifting the latter by modifying the SOP (Sensor Orientation and Position) matrix. Subsequently, the co-registration was refined using the Multi-Station Adjustment (MSA) RiSCAN PRO function. The latter uses an Iterative Closest Point (ICP) method \cite{Zhang1992}. In ICP, the orientation and the position of scan positions is modified using least-squares minimization of residuals in order to calculate the best overall fit in respect to the datum. Each residual is defined as the distance between each data point in the cloud being co-registered and its closest point in the datum. After the best fit is determined, the residual distances were calculated and used to assess the quality of co-registration. For all co-registered scans, the residual distances have a Gaussian distribution with mean of zero. Thus, the precision of the co-registration procedure could evaluated by the standard deviation of the residual distances (σMSA): in our case it ranged from $\pm$0.0598 to $\pm$0.0987 m.

After co-registration, a mask was used to restrict point clouds to the area of interest: the front of the rock glacier and the corridor below. The point density in the area of interest was c. 24 p/m^2 for 2015 surveys and 12 p/m^2 for the 2014 one. The clustering algorithm (DBSCAN) requires as input a point cloud of displacement distance, the latter measured as a Euclidean distance. For any two co-registered datasets, we set the sequentially first dataset as the target and the more recent dataset as the reference. For each point in the target cloud it is necessary to identify its corresponding nearest point in the reference cloud, referred to as the Cloud/Cloud difference (Table 1). Consequently, datasets were compared using the distance tool in the point cloud data management software Cloud Compare software \cite{CloudCompare2012}, freely available at \url{www.danielgm.net/cc}. This tool exploits a chamfer matching algorithm \cite{Barrow1977} to obtain the three-dimensional (Euclidean) distance between each point in the target dataset with its closest point in the reference dataset.

Table 1: LiDAR scans and their use as target and reference dataset in the analyses

Target	**Reference**	**Time-step**
29/06/2015	20/07/2015	1 month
20/07/2015	22/09/2015	2 months
29/06/2015	22/09/2015	3 months
23/09/2014	22/09/2015	1 year

These distances comprise two components: (1) real erosion/deposition signals; and (2) noise associated with the fact that points are not exactly co-located in zones of no change, due to sampling or co-registration errors. In practice, as the MSA used zones of no change, the residual distances for these zones are a measure of the noise in the data (i.e. σMSA). The question then becomes what multiple of σMSA to use. One option is to apply some kind of statistical confidence to the distances

determined (e.g. $\pm 1.96\sigma$MSA gives a 95% confidence that the distance is a signal and not noise, Lane *et al.*, 2003). However, if densities are spatially variable within the zone of interest, or between the zones used for the MSA and the zone of interest, such precision may be misleading. One alternative is to take a process-based definition. Here, we note from field observations that the size of displaced boulders is typically > 0.30 m and we use this as a change criteria: that is a boulder must move through its own volume to be considered a change. For comparison, 0.30 m is approximately 3σMSA, approximately a 99.5% confidence level.

3.4 Choice of DBSCAN parameters

In the present study, the minimum number of points was fixed first, and then the plot of the k-nearest neighbor (k-NN) distance was used to find a suitable value for the *eps* neighborhood size. To test the influence of DBSCAN parameters on cluster identification, the one month scan (Table 1) was used. First, we applied increasing values of *MinPts* (the default of 5, and 10, 15 and 20) to determine the value more appropriate to our case study. We determined k-NN plots for each *MinPts* value, using the plot curvature to identify the optimal *eps*-distance to the k^{th} nearest neighbour. Secondly, to evaluate if the value corresponding to the strong curvature of the k-NN plot is effectively the best choice, we kept *MinPts* equal to the value judged more appropriate (in our case 10) in terms of number of clusters and percentage of noise, and we explored the effects caused by different *eps*-values.

3.5 Determination of erosion and deposition volumes

The DBSCAN algorithm provides a dataset containing the following components: the x,y,z-coordinates of each point plus an integer vector assigning it to either a particular clusters or, for the value 0, as a noise point. For determination of erosion and deposition volumes, a stepwise GIS analysis was performed to classify the points belonging to each cluster as erosion or deposition. This was achieved by using single, rasterized DEMs of the reference data (computed here at 0.5 m resolution) and assigning the sign of the elevation difference to each cluster-point. Each cluster of points was then treated as a data subset. The associated reference and target data points for each cluster were triangulated and the exact volume of change calculated by TIN comparison.

3.6 Comparison with traditional DEM-to-DEM approaches

In a final stage, the results of the cluster-based volume estimates were compared with ones obtained by the traditional, rasterized, DEM comparison approach, focusing on the one month time lapse (June to July 2015). The June and July 2015 co-registered point clouds were interpolated to a 0.3 m regular grid. Given the high point density, a natural neighbor interpolation was deemed sufficient for that purpose. The subtraction between two raster DEMs is traditionally used to detect elevation changes. To isolate real change from noise induced by the data or the interpolation procedure, we followed the error propagation proposed by \cite{Lane2003}, with a 95% confidence limit. The latter

gave a detection limit of ±0.27 m and is very close to the 0.3 m value used for the DBSCAN analysis, hence the detection limit used was rounded up to use the same value.

4 Results

4.1 Effects of DBSCAN parameters

The k-distance graphs obtained by applying *MinPts* equal to 5, 10, 15 and 20 (Figure 5) shows that the related optimal *eps*-values, coinciding with the strong curvature of the plot, also increase from 0.8 up to 1.5 m, approximately linearly. By fixing *MinPts* as equal to 10, values of 0.5, 1.5 and 2 meter for *eps* were tested against the allegedly best one of 1 meter (Figure 5b). Table 2 shows the results obtained by applying these DBSCAN parameters on the number of clusters identified, the percentage of points labeled as noise, the number of movement units detected and the volume of change calculations that result.

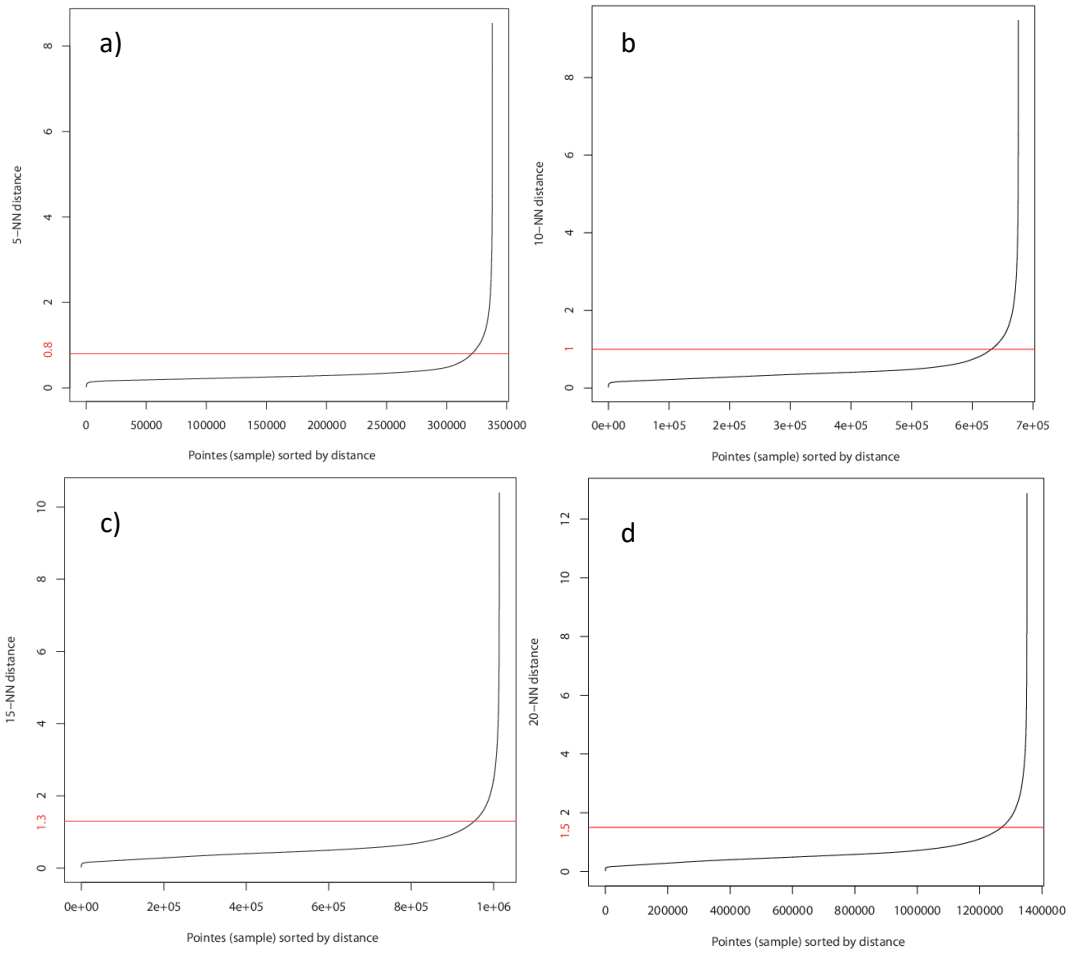

Figure 5. Optimal eps value retrieved using k-NN plots for 5, 10, 15 and 20 MinPts (a, b, c and d respectively).

Table 2 shows that volumetric estimations do not seem to be particularly sensitive to the tested DBSCAN parameters. This is notably the case for the *MinPts* parameter and whilst the number of identified clusters changes substantially, the percentage points classified as noise changes much less. Thus, the effect of *MinPts* is primarily upon the number of clusters identified and not the number of points that become clusters. The number of points that become clusters then is likely to be a key control on the volume estimates. When the *MinPts* is set to 10 and the *eps* parameter is varied, the number of clusters changes dramatically, and so does the percentage of points identified as noise. Thus, the *eps* parameter not only controls the number of clusters identified but also whether seed-point are shared among several clusters, which blend together. It is then not surprising that the volumes of change are more sensitive than when the *MinPts* parameter is varied (Table 2). However, the range of variability of the volume changes is proportionately lower than the range of variability of either the number of clusters or the percentage noise points. That is, a certain number of key points are retained in all analyses, and these have a dominant effect on estimates of volumes of change. It is perhaps interesting that it is the volumes of deposition that are more sensitive to the *eps* parameter and the percentage of points that are noise. This may reflect the fact that the deposition signature is less spatially coherent than the erosion signature, with erosion concentrated on key areas (e.g. the rock glacier terminus) but the deposition reflecting local micro-topography (filling of lows).

The question that then arises is what values, notably of *eps*, should be used? Unfortunately, this analysis gives no clear rule as to what should be chosen, and it does not appear to matter too much for the estimation of erosion on this surface. For deposition, the only means of providing a justification is to consider the spatial scale of the kinds of depositional process that has been observed in this kind of environment. Deposition appears to be micro-topography controlled, with a length scale of about 1 m, suggesting a 1 m value of *eps*. More generally, use of this kind of approach needs additional field observations to help to choose the most suitable value of the *eps* parameter according to the expected scales of erosion and deposition.

Table 2: Sensitivity of the resulting number of clusters and volumes of erosion and deposition to changes in the DBSCAN parameters. (Parameter setting as in Figure 6)

Parameter setting	**MinPts***	**Eps [m]**	**Cluster features**	**Noise points (%)**	**Detected movements**	**V_{TOT} [m^3]**	**V_E [m^3]**	**V_D [m^3]**
	(*increasing)							
a) 1	5	0.8	695	5.0	913	761	320	441
a) 2	**10**	**1**	**327**	**6.8**	**484**	**738**	**313**	**425**
a) 3	15	1.3	159	6.3	261	748	316	432
a) 4	20	1.5	108	6.5	185	747	315	432
	(*constant)							
b) 1	10	0.5	751	22.7	814	658	290	368
b) 2	**10**	**1**	**327**	**6.8**	**484**	**738**	**313**	**425**
b) 3	10	1.5	149	2.7	241	788	330	458
b) 4	10	2	86	1.3	148	808	338	470

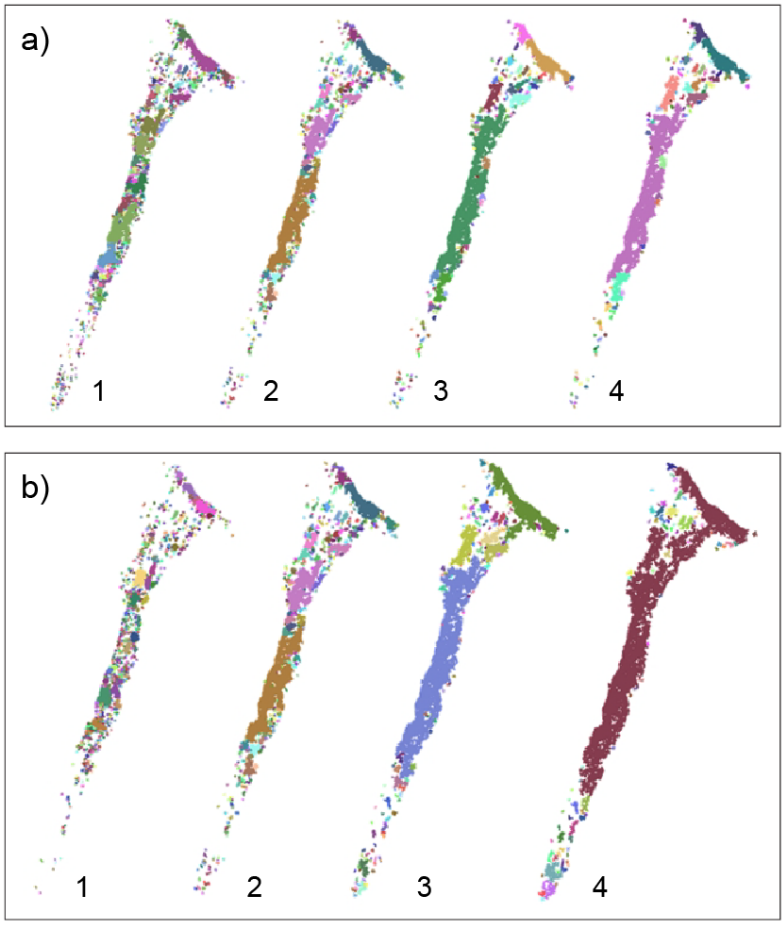

Figure 6. Sensitivity of the clusters aggregation/disaggregation to changes in the DBSCAN parameters (see Table 2).

4.2 Comparison with traditional DEM comparison

Figure 7 compares the maps of erosion and deposition clusters obtained with DBSCAN with the results obtained using a traditional, rasterized, DEM comparison. At one level, the patterns are very similar. The same areas are highlighted as erosion and deposition, although the rasterized DEM of difference has more scattered, isolated changed as the comparison makes no reference to the extent to which the data are coherently organized. However, volumetric estimations are three times higher than the 3-D point cloud approach (see Table 3 below), with values for one month close to what would be expected to be observed in one year. These volumetric changes appear unrealistic at the timescale of one month for the presented case study. We attribute this to the effect of artificial surface differences associated with point density effects. Point interpolation assigns an elevation to every grid point and then every grid point is compared, giving a change if it is greater than the 0.30 m detection limit used here. No reference is made to the coherence of changes by reference to adjacent points. Given complex surface variability, interpolation to grids may cause isolated elevation changes that are a result of the chance inclusion of topographic highs and lows in the interpolation surface, rather than any actual geomorphic change. More generally, whether or not a DBSCAN style algorithm is used, meaningful detection of surface change should consider the spatial coherence of the change, with respect to the known spatial variability within the surface.

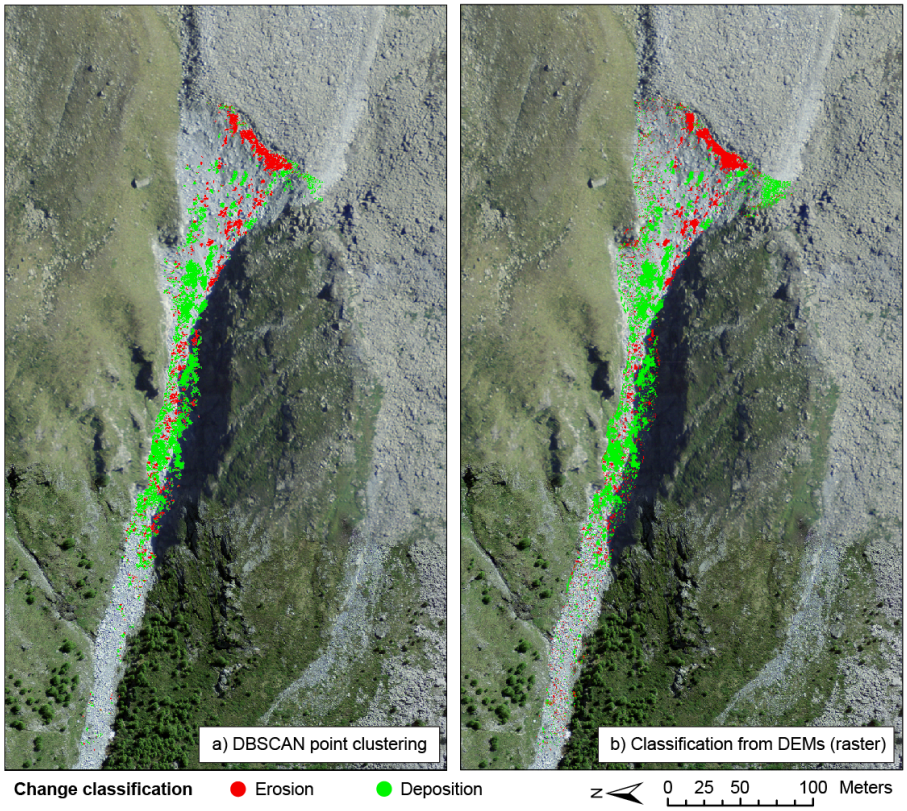

Figure 7: Comparison for one month data between a) DBSCAN point clusters and b) erosion and deposition patters classified from rasterized DEMs comparison.

5 Discussion

5.1 Merits of a 3D-clustering approach

Remote sensing techniques for data acquisition have developed rapidly in recent years. The output of these procedures, 3D point clouds, are widely used in the geosciences (Abellan et al. 2016) and developing new and fast algorithms for feature extraction is mandatory in this context. Our approach, based on a density clustering method, proved to be very useful for detecting movement units (i.e. erosion and deposition features) at a rock glacier front, allowing extracting and quantifying volumetric changes. The same procedure can be applied to extract 3D features related to any geomorphologic process such as rockfall, debris flows, landslide, etc. As with similar methodologies based upon using point clouds for feature detection (Riquelme 2014, Tonini 2014, Olsen 2015), our approach leads to a reduction in noise and to the clustering single points into individual features. Nonetheless, compared with existing applications, there are some advantages. First, it is very fast, notably with the most recent version of the DBSCAN package (Hahsler et al. 2016). Second, by adopting a 3D approach, the method can be applied to any surface regardless of local topographic slope. On steep mountain sides, lateral point displacement may be reduced, with vertical point displacement becoming important, emphasizing the need for a 3D rather than a 2D approach. Third, the proposed methods allowed the isolation of clusters directly from point clouds without the prior need for interpolation or data reduction and with an accuracy that depends only on the actual sampling resolution.

5.2 Geomorphological activity at the rock glacier front

Figure 8 illustrates the clusters identified by DBSCAN, where each color corresponds to a unit of morphological change. The geomorphological activity during one month in the summer 2015 highlights a major cluster with diverse smaller ones at the rock glacier front (Figure 8a, 1). From 100 m downslope, an area of deposition is characterized by the presence of two particularly large clusters (Figure 8a, 2). In the lower part of the area of study, very small clusters are observed (Figure 8a, 3). These are likely to be single boulders that were able to move farther downslope in the channel.

Clusters identified over a three month period (Figure 8b) appear larger at the rock glacier front, although they do not seem to be more numerous. Despite their proximity, the two major clusters are not unified (Figure 8b, 4). The central part of the slope seems slightly more fragmented, although two very large clusters are once again visible (Figure 8b, 5). Larger clusters are featured in the lower part of the study area in comparison with the shorter timescale analysis, indicating that several boulders reached that zone (Figure 8b, 6).

One-year clusters are shown in Figure 6c. Almost the whole front surface has undergone change, as indicated by various large clusters (Figure 8c, 7). The middle part of the area of interest has almost completely changed as well, as testified by the presence of many clusters including a very large one (Figure 8c, 8). In the lower part, small clusters precede another very large one, depicted in green (Figure 8c, 9).

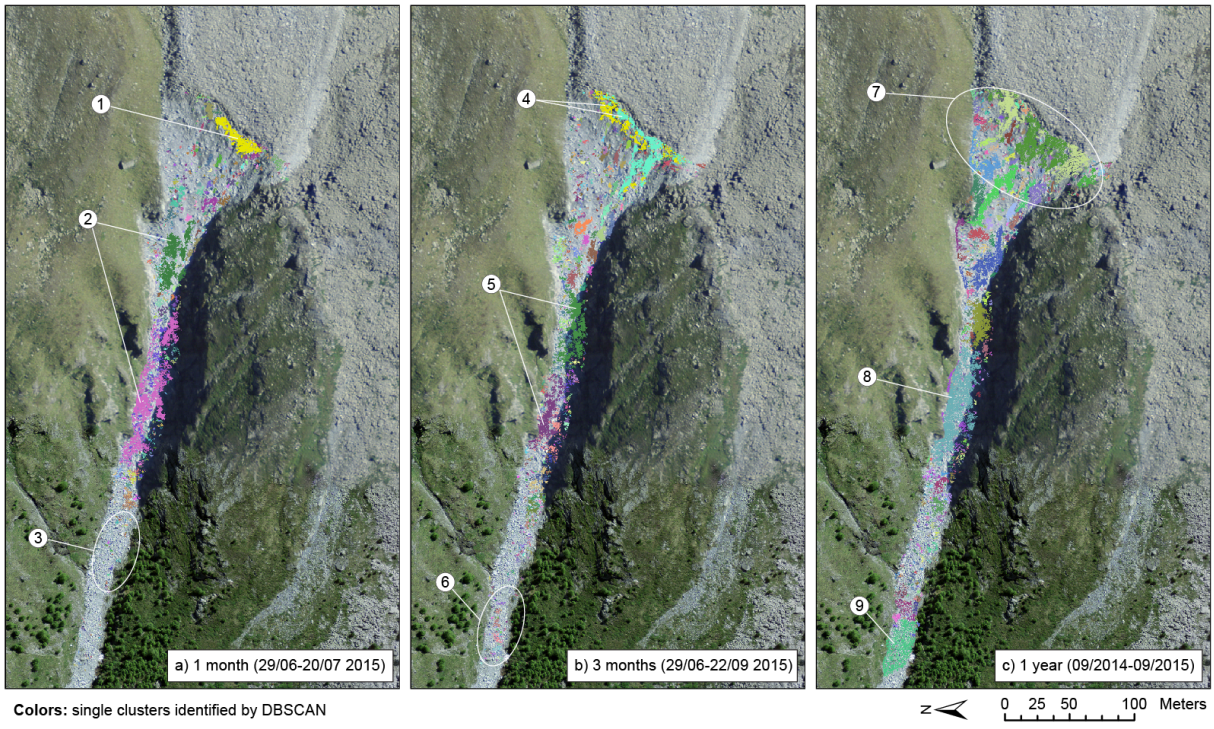

Figure 8: Three-dimensional geomorphological changes identified using DBSCAN for a) one and b) three months and c) one year time lapses. The color of the dots represents single erosion or deposition features. Numbers are referred to in the text.

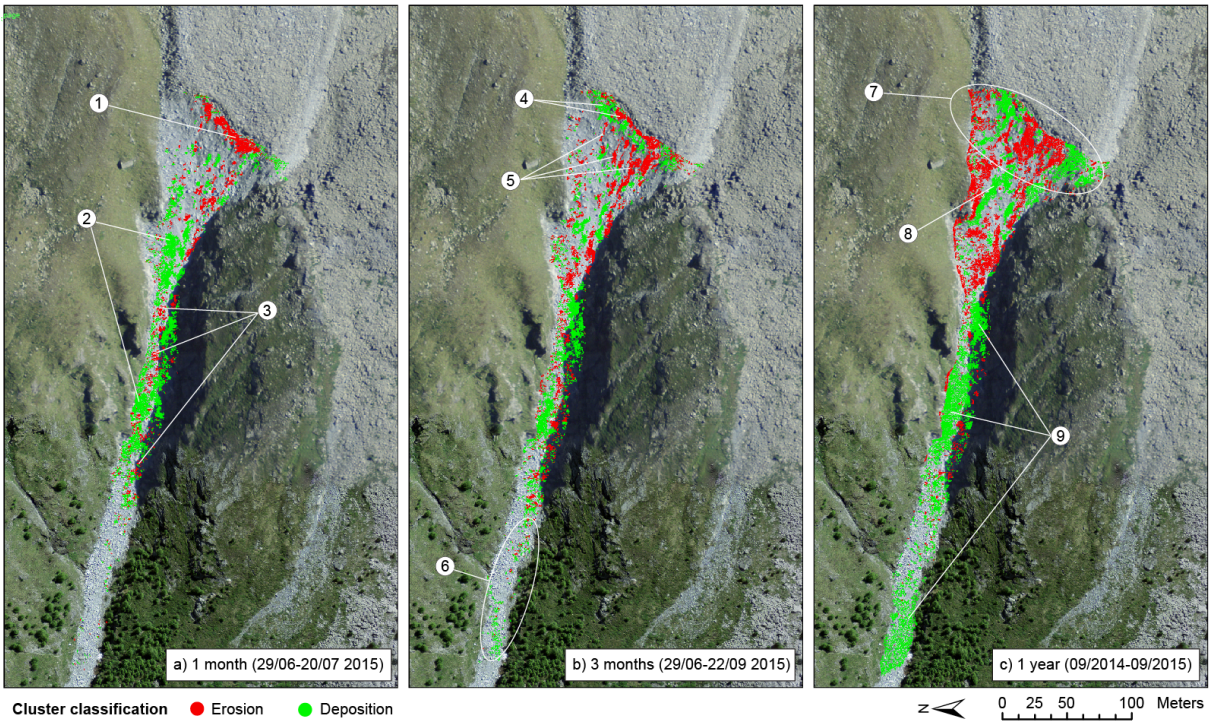

Figure 9: Deposition and erosion features for the field campaigns corresponding to a) one and b) three months and c) one year time lapses.

The clusters presented in Figure 8 are classified as erosional or depositional following the procedure discussed in Section 3.4 (Figure 9). This demonstrates that the largest cluster visible at the front at the one-month time-step is due to a collapse event which occurred in July 2015 (Figure 7a, 1). The remaining features in this zone are a mixture of erosion and deposition, probably caused by detached material blocked by other boulders and unable to travel farther. As expected, the vast majority of clusters in the channel are depositional (Figure 9a, 2). Erosional footprints in that zone are scattered but exist (e.g. Figure 9a, 3), indicating potential remobilization of material or incision.

Figure 9b shows that the two major and separated front clusters at the three month time-scale are opposite in nature (Figure 9b, 4). The fact that the erosional cluster is located above the deposition area allows two hypotheses. On the one hand the eroded material could have simply slid from the upper part of the detachment niche without leaving the rock glacier front. On the other hand, the two clusters could be unrelated; in that case the eroded material has likely left the front area, and the depositional pattern could be due to the front advance caused by deformation-related creep in the rock glacier body. Given the scale of analysis (three months) and the seasonal conditions (summer, affected by a heat wave), this second scenario appears more realistic. The front is also characterized by the presence of many erosional clusters with elongated shapes (e.g. Figure 9b, 5), very likely caused by collapse and consequent transit of material downstream. Spatial patterns in the channel are similar to the one-month application, but material is deposited further downstream in this case (Figure 9b, 6).

The geomorphological activity at the rock glacier front over one year is almost equally divided into erosion and deposition (Figure 9c, 7). Whilst erosional patterns are proof of material collapsing as permafrost thaws, the green features in Figure 7c are probably due to the rock glacier advancing. In that sense, deposition in these clusters is only apparent, as it is merely a displacement forward.

Starting from only 50 m below the crowning of the front, depositional patterns could also be caused by material trapped after a collapse by cause of surface roughness; the elongated cluster in the center could be an example (Figure 9c, 8). Throughout the course of the channel, large clusters of deposition are visible (Figure 9c, 9).

Table 3: Synthesis of the geomorphological activity (deposition (D) and erosion (E) movements) at the Tsarmine rock glacier during the summer 2015 and between Sept. 2014 and Sept. 2015. Volumes (V) in m^3.

Time-step	**Number of clusters**	**V_{TOT} [m^3]**	**V_E [m^3]**	**V_D [m^3]**
1 month	484	738	313	425
2 months	543	826	410	416
3 months	410	1376	536	840
1 year	538	2056	724	1332
1 month (traditional DEM comparison)	-	2079	1014	1065

Table 3 summarizes the geomorphological activity at the Tsarmine rock glacier during the summer 2015 (one, two and three month time-steps) and during one entire year (September 2014 to September 2015). The number of clusters identified by the DBSCAN analysis oscillates between 410 and 543 and does not seem to be related to the duration considered. On the other hand, the total volume of geomorphological change (V_{TOT}) consistently increases as time intervals increase. This implies that over the longer term bigger clusters of geomorphological activity are being identified, which is the expected outcome, also reflected in no real evolution in the number of clusters. Generally, estimates of eroded and accumulated volumes are balanced at short time scales (one and two months), as one would expect. However, deposition volumes dominate at the longer time span. A possible explanation lies in the fact that the front invariably advances under the influence of creep-realted deformation in the rock glacier body. The process is slow and continual, and permafrost thaw and rock fall at the front mitigates it, but at longer timescales it is possible that a part of the front has not yet collapsed, and the advance become visible as an apparent gain of material. On the other hand, another consequence is the reduction or suppression of the volumes of collapsed material that can be observed, as the void might be masked by front advance. Consequently, results should tend to slightly overestimate the total accumulation and underestimate eroded volumes. These processes are likely to be relevant at intermediate and long timescales (e.g. three months and one year, Figure 9b and 9c), and explain (i) the unbalance between V_E and V_D at these timescales, and (ii) the disagreement between the combination of eroded volumes (V_E) for one and two months and three months erosion.

\cite{Meteoswiss2016}, in their annual climatic report, indicated that year 2015 was, after the remarkable years 2011 and 2014, once again a record-year for measured air temperature. In particular, the summer 2015 was characterized by an extreme heat wave, and it is classified as the second warmest summer in Switzerland since the beginning of measurements, 152 years ago. Beaten only by the extreme summer of 2003, it registered 2.7 °C more than the norm 1981-2010 \citep{Meteoswiss2016}. As a permafrost-related process, rock glacier creep is supposedly very

sensitive, amongst others controlling factors, to temperature forcing (e.g. \cite{KellererPirklbauer2012}). The results achieved in this study offer detailed information on the dynamics of the Tsarmine rock glacier front during the hot summer of 2015. During only about one month, 313 m^3 of erosion occurred in the investigated zone. The following two months display slightly higher values: 410 m^3. For both periods, little more than 400 m^3 of accumulated material are estimated. The superior geomorphological activity in the shorter, earlier time span could be an indication of the crucial role of snowmelt, which generally occurs around June for this elevation and orientation, in eroding and mobilizing boulders at the rock glacier front. Another reason could be a strong capacity of thawing at the front that manifests at the beginning of the summer season.

Analysis of the June and September 2015 LiDAR datasets resulted in an estimated 536 m^3 of erosion. It could be argued with confidence that this result is an underestimation. GPS measurements indicate that the rock glacier surface moved at a velocity of almost 5 myr^{-1} during that period, which correspond to a net advance of 1.25 m. This process partially conceals collapse events by causing the front to advance and occupy the space left empty. The volume of eroded material should be at least a few hundred cubic meters more. The same is true for volumetric estimations for one year (September to September). We argue that erosion quantities (724 m^3) are strongly underestimated for the same reason, as confirmed by accumulation volumes that are almost double of them (1332 m^3, excluding material that traveled further downstream). Whilst an accurate estimation could not be formulated, it is realistic to assume that the rock glacier front delivers sediments downstream in the order of c. 1500 m^3yr^{-1}.

The mass transfer occurred at the Tsarmine rock glacier front during the hot summer 2015 appears extremely high, a fact that could be attributed to the exceptionally high mean velocities observed in the last couple of years (c. 4 myr^{-1}). These are considerably higher than the kinematics estimated for the beginning of the 2000s (1-2 myr^{-1}, Barboux et al 2014, Micheletti et al 2015), which nonetheless included the 2003 heat wave, suggesting that sediment delivery rates might be much higher nowadays in comparison with 10-15 years ago. In this regard, Roer et al. (2012) observed, for a very active rock glacier located in an adjacent valley (the Turtmann Valley), maximum velocities of 2.59 myr^{-1} during the heat wave of the summer 2003, with a corresponding peak of sediment transfer rate of 1.1 Mt yr^{-1} (corresponding to c. 415 m^3yr^{-1} if a specific weight of 2.65 t m^{-3} is considered, Barsch 1977). For a similar case study in the Mattertal Valley, Lugon and Stoffel (2010) encountered much slower kinematics at the beginning of the years 2000s, with maximum movement rates of 0.88 myr^{-1}. They estimated a mass flux of 500-700 m^3yr^{-1}, but corrected sediment delivery to 300-400 m^3yr^{-1} due to the considerable amount of voids and ice contained in the rock glacier. Following these indications, it would be plausible to assume that erosion volumes at the Tsarmine rock glacier have almost doubled in the last decade. Comparing our results to the behavior of other rock glaciers during the hot summer of 2015 could provide insights in this sense.

The maps of erosion and deposition clusters (Figures 8 and 9) illustrate how the front line position of the rock glacier did move significantly during the period of study. Boulders detaching from the front do not appear to travel far. Large clusters of deposition are identified a few hundred meters below the front, and with a few exceptions at longer time spans where traces of material extend farther downstream, boulders are exclusively stocked in the first 200 m of the channel. Hence, despite evidence of significant sediment production at the rock glacier front, impacts at the valley bottom

are absent for the time being. A further remobilization of this material (e.g. by debris flows events) is not to be excluded, but the diameter of rocks is quite substantial and thus the risk quite mitigated.

5 Conclusions

The application of the DBSCAN 3D-module using LiDAR point clouds permitted detection of erosion and deposition features, their mapping and derivation of detailed volumetric change estimations for a rock glacier front located in the Swiss Alps. Single clusters of erosion and deposition were extracted directly from point clouds without the necessity of reduce or interpolate the 3-D original data. The proposed approach is semi-automatic and allows detecting realistic volumetric features, depending only on the actual data available. This methodology represents an alternative to traditional point cloud processing techniques for applications in geomorphology.

Remarkable geomorphological activity was observed at a rock glacier front during the summer of 2015, likely under the influence of the very rapid permafrost creep suggested by GPS measurements. To determine if the influence of the exceptionally high temperatures observed that season plays a driving role in these processes, TLS surveys for the following summers would be necessary, and the proposed approach would be ideal to efficiently process the resulting datasets. Moreover, a more detailed coupling between meteorological events, climatic data and morphological changes were beyond the focus of this study, but would need to be performed to infer the effects of external forcing on sediment production at a rock glacier front.

\section*{Acknowledgments}

This research was supported by the Herbette Foundation of the University of Lausanne, the Canton Vaud, and the Canton Valais. We are very grateful to the Universities of Lausanne and Fribourg for funding the laser scanner device used in this study. We would like to thank Mario Kummert and Adnan Tahir for their valuable help in the field.

References to add in bibtex

Ester, M., Kriegel, H.-P., Sander, J., and Xu, X. 1996. A density-based algorithm for discovering clusters in large spatial databases with noise. Proc. 2nd Int. Conf. on Knowledge Discovery and Data Mining. Portland, OR, pp. 226-231.

Campello, R. J. G. B.; Moulavi, D.; Sander, J. (2013). Density-Based Clustering Based on Hierarchical Density Estimates. Proceedings of the 17th Pacific-Asia Conference on Knowledge Discovery in Databases, PAKDD 2013, Lecture Notes in Computer Science 7819, p. 160.

Reference R:

@Manual{title= {R: A Language and Environment for Statistical Computing}, author= {{R Core Team}}, organization = {R Foundation for Statistical Computing}, address = {Vienna, Austria}, year = 2015, url = {https://www.R-project.org}}

Dbscan package ref:

Hahsler et al 2016 (see pdf)